Finite-element simulations of Al7075-T6 orthogonal cutting: Effect of part geometry and mesh on chip morphology and formation mechanism

Cite as: AIP Conference Proceedings **2113**, 080003 (2019); https://doi.org/10.1063/1.5112611
Published Online: 02 July 2019

Mehdi Benhassine, Edouard Rivière-Lorphèvre, Pedro-Jose Arrazola, Pierre Gobin, Aurélie Granjon, Ohian Aizpuru, and François Ducobu

Finite-Element Simulations of Al7075-T6 Orthogonal Cutting: Effect of Part Geometry and Mesh on Chip Morphology and Formation Mechanism

Mehdi Benhassine[1, a)], Edouard Rivière-Lorphèvre[1], Pedro-Jose Arrazola[2], Pierre Gobin[3], Aurélie Granjon[3], Ohian Aizpuru[4] and François Ducobu[1]

[1]*Machine Design and Production Engineering Lab, Faculty of Engineering, University of Mons (UMONS). Place du Parc 20, 7000 Mons BELGIUM.*
[2]*Mechanical and Manufacturing Department, Faculty of Engineering, Mondragon University. 20500 Mondragon SPAIN.*
[3]*Sobelcomp SPRL. Rue de l'économie 13, 4431 Loncin BELGIUM.*
[4]*Zubiola. Poligono Basterretxe, 20720 Azkoitia (Gipuzkoa) SPAIN.*

[a)] Corresponding author: mehdi.benhassine@umons.ac.be

Abstract. Machining of aluminum alloys is of great interest for the aeronautical industry. Amongst those, the Al7075-T6 alloy remains a major component. Numerical studies of the orthogonal cutting of such alloys present a few challenges. One of them seems to be the absence of a unified way to capture the chip morphology without artificially modifying the mesh or the piece geometry to facilitate a segmented chip formation. It is accepted that Al7075-T6 forms segmented chips for typical industrial cutting speeds. In this contribution, a FEM model with a structured mesh is used with the commercial code Abaqus/Explicit v6.14 in the Lagrangian scheme. With this straight-forward approach, it is possible to reproduce the cutting forces and the chip morphology obtained in practical cases. The results are validated against experimental tests found in the literature.

INTRODUCTION

The interest of the Aluminum in the aerospace industry is clear. Lightweight, good corrosion resistance and mechanical properties make this material central to almost all aircraft designs. In this study, the Al7075-T6 variant is used [1]. It offers slightly better corrosion resistance than the other main Al alloy for aeronautical applications, the Al2024. The optimization of machining for Al7075-T6 is important when precision is required. It is well accepted that segmented chips are formed at industrial cutting speeds. This is observed both experimentally [2-3] and in numerical studies [4-5]. In simulations, authors are using separate zones in the cut region, the uncut chip material zone (UCMZ) and the machining affected zone (MAZ). Both regions exhibit the same constitutive parameters but the fracture energy for the MAZ region is lower reflective of the mode II fracture mechanism rather than mode I for the UCMZ. Ahead of the tool tip, the Al material fracture is essentially made via crack opening, whereas ahead of the tip, shearing is responsible for material removal [3]. Numerical results are available for negative angles, and experiments are available for positive and negative rake angles but less is known for Al7075 compared to Ti6Al4V.

In the contribution, a straight-forward approach tends to unify some formalisms and model definitions to remove numerical artifacts as much as possible making no a-priori assumptions on piece geometry or mesh structure.

Proceedings of the 22nd International ESAFORM Conference on Material Forming
AIP Conf. Proc. 2113, 080003-1–080003-6; https://doi.org/10.1063/1.5112611
Published by AIP Publishing. 978-0-7354-1847-9/$30.00

MODEL

The AL7075-T6 constitutive model is the Johnson-Cook (J-C) model. Its following stress-strain relationship is given as

$$\sigma = [A + B\varepsilon^n]\left[1 + C ln\frac{\dot{\varepsilon}}{\dot{\varepsilon}_0}\right]\left[1 - \left(\frac{T-T_0}{T_m-T_0}\right)^m\right] \quad (1)$$

Where σ is the plastic stress, ε is the strain, $\dot{\varepsilon}$ is the strain rate. $\dot{\varepsilon}_0$ is the reference strain rate (1 s^{-1}) and T is the temperature; A, B, C, T_0 and m are model constants. A is the initial yield stress, B is the hardening modulus, n is the strain-hardening exponent. C is the strain-rate dependent coefficient, m is the thermal softening coefficient and T_0 is the transition temperature. The model constants are reported in table 1. The tool was treated as an analytical rigid body. To consider element deletion, the J-C fracture model was employed. The fracture model is responsible for the segmented chip formation as localized strain accumulation occurs at the tool tip. A cumulative damage law was employed whereas the damage parameter D (equal to 1 at failure) was defined as:

$$D = \sum \frac{\Delta\bar{\varepsilon}}{\varepsilon_f} \quad (2)$$

With the cumulative plastic strain $\Delta\bar{\varepsilon}$ and the strain at failure ε_f given as

$$\varepsilon_f = \left[D_1 + D_2 e^{\left(D_3\frac{p}{q}\right)}\right]\left[1 + D_4 ln\frac{\dot{\bar{\varepsilon}}}{\dot{\varepsilon}_0}\right]\left[1 - D_5\left(\frac{T-T_0}{T_m-T_0}\right)^m\right] \quad (3)$$

p is the pressure stress and q is the Mises stress. D_1, D_2, D_3, D_4, D_5 are fitting constants of the model (with no dimension). When damage initiation occurs, its evolution is given as a linear softening law with two different fracture energies for the UCMZ (the chip formation above the crack tip consists of opening analogous to mode I fracture (with a value of 9.51 mJ/mm² corresponding to a K_I of 29 MPa √m [6]) whereas, in the machining affected zone, shearing is occurring as the tool tip cuts the material (a lower value of 7.06 mJ/mm² corresponding to a K_{II} value of 25 MPa√m [7]).

TABLE 1. Johnson-Cook constitutive model constants and damage constants for Al7075-T6 [5,6].

Constant	Value	Constant	Value
A (MPa)	546	D_1 (-)	-0.068
B (MPa)	678	D_2 (-)	0.451
C	0.024	D_3 (-)	-0.952
n	0.71	D_4 (-)	0.036
m	1.56	D_5 (-)	0.697
T_m (K)	893		
T_0 (K)	300		

The orthogonal cutting model consisted of an Al7075-T6 solid meshed with 4-node isoparametric elements with temperature and bilinear displacement (CPE4RT). Abaqus/EXPLICIT v6.14 in the Lagrangian scheme was used. Hourglass was set to Relax stiffness following the recommendations of Jomaa et al [5]. The interaction followed a Coulomb friction model with the adjunction of heat generation at the interface with a standard 50% dissipation between the tool and Al piece. Distortion control has been set to 0.5 for all simulations.

The Al part was meshed with 5 µm squared elements in both Zones A and B (see Fig. 1 (a) and (b)). The rest of the part was meshed with 5x10 µm rectangular elements. The mesh was not angled at 45° like Ye et al [8] or other numerical studies stating that the segmented chip formation is greatly enhanced with a structured angled mesh [3-4, 6]. Other authors also change the part geometry by having a notch shape [3-4]. This modification aimed at facilitating the chip segmentation is not necessary as shown in the results section. This approach presents the originality of our model.

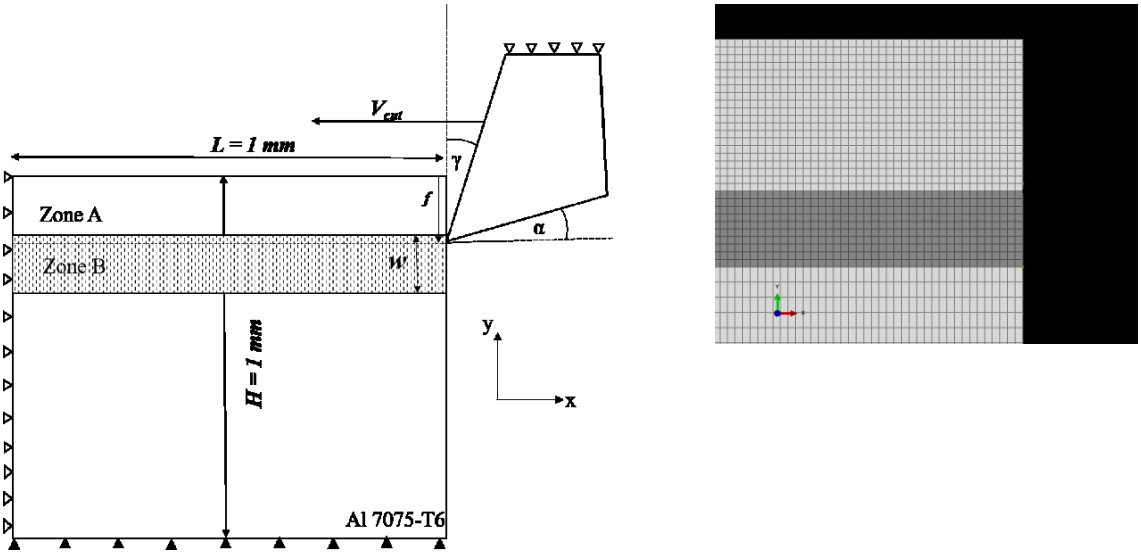

Figure 1. (a) Al 7075-T6 orthogonal cutting model the Zone A represents the Uncut Chip Material Zone and Zone B is the Machining Affected Zone. γ and α are respectively the rake and relief angles. f is the feed, V_{cut} is the cutting speed and w is the width of the machining affected zone. (b) View of the mesh.

Model Validation

To validate the model, reaction forces were compared to the orthogonal cutting tests performed by Daoud with the same cutting conditions [4]. A comparison of the chip formation mechanism between this study and the numerical study of Jomaa et al [5] was also made.

The segmented chip formation mechanism is accepted to occur in three stages [4-5], strain localization leading to shear banding and adiabatic shear banding initiation leading to chip formation. Fig. 2 shows that our model was able to reproduce these stages.

The cutting forces comparison with the experiment is shown in Table 2. The reference [4] gives experimental values for a piece of 3.14 mm width with a relief angle of 11° and a 0° rake angle at 931 m/min.

TABLE 2. Comparison between Al 7075-T6 orthogonal cutting tests [4] with current numerical model. RMS values were calculated once the tooltip started to come in contact with the workpiece.

Cutting Speed V_{Cut} (m/min)	**Experimental Cutting Force (N/mm) [4]**	**Experimental Feed Force (N/mm) [4]**	**Cutting Force F_c (N/mm)**	**Feed Force F_n (N/mm)**
931	127.8	34.1	126.6 ± 7.9	18.2 ± 4.8

The comparison between cutting forces was very close to the experimental value, whereas the feed force was under-estimated. This underestimation was also obtained by the reference's numerical results [4] falling within 20% of the measured feed forces. It is therefore safe to assume that the model is validated as the cutting force is the most important value of interest in orthogonal cutting. Furthermore, the validation test showed that the formation mechanism, and shear planes were similar with AL7075-T651 at negative rake angles.

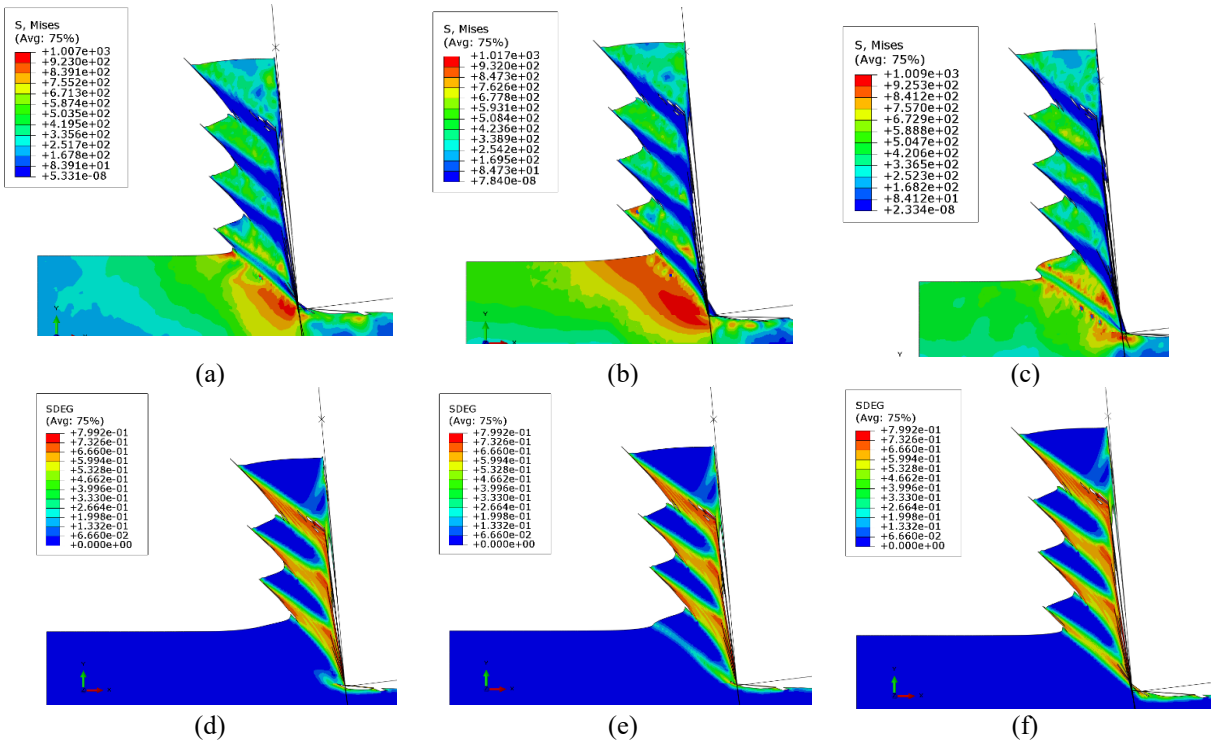

FIGURE 2. The three stages of chip formation in Al7075-T6. (a), (b) and (c) present the stress distribution during the chip formation process. (d), (e) and (f) show the degradation parameter.in (d), strain localization at the tool tip is followed (e) by adiabatic shear banding leading to (f) segmented chip formation.

RESULTS AND DISCUSSION

Reaction Forces

With the validated model, the parameter space was chosen as followed in Table 3.

TABLE 3. Parameters employed in simulations

Simulation Parameter	Value
Feed, f (mm/rev)	0.15
Cutting Speed, V_{Cut} (m/min)	156, 650, 1144
Rake angles, γ (°)	-5, 5
Clearance angle, α (°)	7
Hourglass setting	Relax Stiffness
Machined zone width (mm)	0.1

For both negative and positive rake angles, the cutting forces presented a jigsaw pattern characteristic of segmented chip formation [5, 9]. Chip segmentation was observed in all cases of the parameters studied, and chip separation was more important with the negative rake angle. Cutting and feed forces values are presented in Table 4.

TABLE 4. Root Mean Square values of reaction forces with standard deviation for the different combination of cutting speeds and rake angles. A constant relief angle of 7° was used throughout as well as a 0.15 mm feed.

Cutting Speed (m/min)	Rake Angle (°)	Cutting Force Fc (N/mm)	Feed Force Fn (N/mm)
156	-5	130.1± 14.6	43.9 ± 16.4
650	-5	125.4 ± 16.6	41.2 ± 14.9
1144	-5	133.7 ± 21.0	29.8 ± 8.9
156	5	109.2 ± 8.0	10.0 ± 3.3
650	5	108.2 ± 5.5	9.2 ± 3.5
1144	5	107.5 ± 6.5	8.6 ± 3.3

The cutting forces were slightly increasing linearly with the cutting speed with the negative rake angle, but a reduction of magnitude was observed for positive angles and for the range of speeds studied, no clear trend was found as the standard deviation was higher in the case of the negative rake angle and more investigation in needed to understand this issue. Daoud et al present the shortcomings of Johnson-Cook models to predict cutting forces since the microstructure is not taken directly into account but only strain, strain rate and temperature and the strain rate is independent with temperature which may not occur for metals [4]. Smaller forces are expected for positive angles in typical metal experiments. It is stressed here that our model provided the same results with no a-priori hypothesis on piece geometry or mesh. The feed and reaction forces were lower with a positive rake angle.

Chip Morphology

The chip morphology depended on the two rake angles studied, the negative rake angle favored easier chip separation from the rake face than the positive angle, as seen on Fig. 3. This separation was increased with higher cutting speeds. The positive rake angle accompanied a less segmented chip throughout the cutting process for the three cutting speeds used.

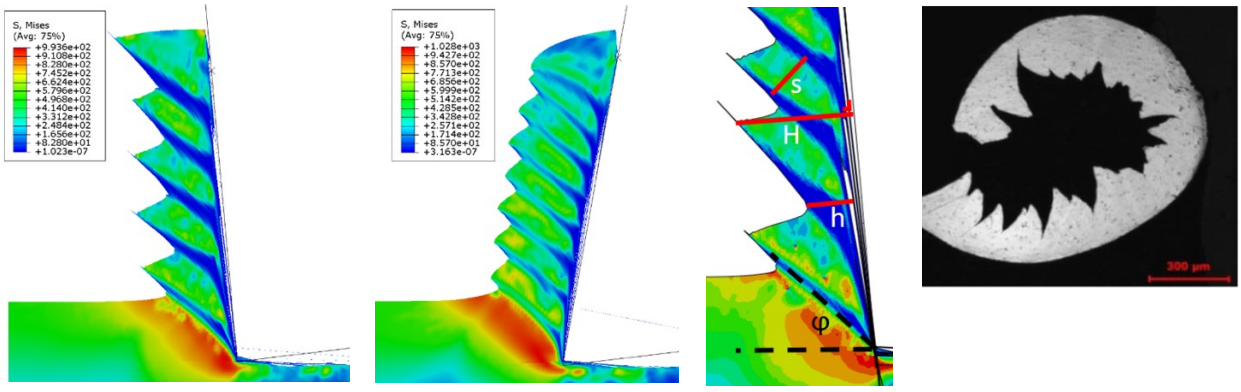

(a) (b) (c) (d)

Figure 3. Segmented chip formed at 156 m/min with a -5° rake angle (a) and 5° angle (b). Von-Mises stress values in MPa are also displayed. (c) Geometrical parameters for chip morphology definitions. Shear Angle φ, continuous chip length *h* taken normally to the rake face, the height of the chip *H* and the shear band spacing *s*. (d) presents typical AL7075-T6 chips as shown in reference [4] for 650 m/min at 0° rake angle and a feed of 0.16 mm.

To quantify the chip morphology and compare to found experiments in ref [5], the definition of Jomaa et al was used. Although the tests in this reference are for Al 7075-T651, the morphology details are presented for a semi-quantitative comparison. The chip curl in part (d) may be the result of cooling after the machining process. The results are reported in table 5.

At 1144 m/min, with a -5° rake angle, the average chip shear angle was 35.7° compared to 38° in the experimental data in [5] for Al 7075-T651. The continuous chip length was measured at 0.146 mm while the height of the chip measured 0.184 on average giving a segmentation intensity of 0.759 which was closer to the 156 m/min tests in reference [5]. Shear band spacing was measured at 0.076 mm.

TABLE 5. Geometrical characteristics of the segmented chips. Mean values are presented with the standard deviation. The population for each set of measurements is 10 segments of the same chip. Results from experiments on Al 7075-T651 of Jomaa [5], measured from the graph plots in the reference, are given as a qualitative comparison.

Cutting Speed (m/min)	Rake Angle (°)	Shear Angle φ (°)	Continuous Chip Length h (mm)	Height of the Chip H (mm)	Segmentation intensity h/H	Shear Band Spacing s (mm)
156	-5	38.2 ± 1.6	0.079 ± 0.005	0.133 ± 0.008	0.600 ± 0.053	0.026 ± 0.004
156 [5]	-5	27	0.17 ± 0.09	0.3 ±0.05	0.58	0.125 ± 0.073
650	-5	36.1 ± 1.4	0.072 ± 0.007	0.134 ± 0.006	0.543 ± 0.038	0.033 ± 0.005
650 [5]	-5	31	0.10 ± 0.05	0.25 ± 0.05	0.45	0.125 ± 0.06
1144	-5	35.7 ± 1.7	0.146 ± 0.003	0.0.184 ± 0.008	0.759 ± 0.031	0.076 ± 0.015
1144 [5]	-5	38	0.065 ± 0.015	0.20 ± 0.05	0.3	0.09 ± 0.01
156	5	26.99 ±4.3	0.123 ± 0.016	0.153 ± 0.09	0.800 ± 0.089	0.097 ± 0.021
650	5	42.0 ± 2.0	0.088 ± 0.004	0.122 ± 0.005	0.715 ± 0.042	0.026 ± 0.005
1144	5	44.57 ± 2.0	0.080 ± 0.003	0.124 ± 0.002	0.648 ± 0.029	0.075 ± 0.009

CONCLUSION

Finite-element simulations of orthogonal cutting have been realized for Al 7075-T6. A squared elements mesh was created with a realistic consideration of fracture according to other recent numerical studies. After a comparison with experimental and numerical data from the literature, the model was validated and served to provide insights on the effect of the rake angle on cutting forces and chip morphology. From this study and as expected from practical tests, the chips detach more easily from the rake face when the rake angle is negative than in the positive inclination. The complete chip is less serrated when the rake angle is positive. The same results as what is expected in machining tests of Al 7075-T6 are recovered by the model. The reaction forces are lower for positive angles than negative angles. The present model will be used in conjunction with composites for stacks in a future contribution.

ACKNOWLEDGMENTS

The authors acknowledge the Région Wallonne (Belgium) for funding under Convention N° 1610039.

REFERENCES

1. *"Metals Handbook, Vol.2 - Properties and Selection: Nonferrous Alloys and Special-Purpose Materials*", (ASM International 10th Ed.,1990).
2. A.R. Torabi, F. Berto and A. Campagnolo, Phys Mesomech **19** (2), 204-214 (2016).
3. T. Mabrouki, F. Girardin, M. Asad, J. Rigal, Int J Mach Tool Manu **48**, 1187-1197 (2008).
4. M. Daoud, W. Jomaa, J.F. Chatelain and A. Bouzid. Int J Adv Manuf Technol **77** (9-12), 2019-2033 (2015).
5. W. Jomaa, O. Mechri, J. Lévesque, V. Songmene, P. Bocher and A. Gakwaya, J Manu Process **26**, 446–458 (2017).
6. N.S. Brar, V.S. Joshi and B.W. Harris, AIP Conf. Proc. **1195**, 945 (2009).
7. T.K. Todkari, M.C. Swami and P.S. Patil, IOSR JMCE **12** (1); 01-05 (2015).
8. G.G. Ye, Y. Chen, S.F. Xue and L.H. Dai, Int J Mach Tool Manu **86**, 18-33 (2014).
9. F. Ducobu, E. Rivière-Lorphèvre and E. Filippi, Int J Mech Sci **81**, 77-87 (2014).